https://doi.org/10.5194/bg-2022-228
Preprint. Discussion started: 25 November 2022

Biogeosciences Discussions

Assessing global-scale organic matter reactivity patterns in marine sediments using a lognormal reactive continuum model

Sinan Xu[1,2], Bo Liu[2], Sandra Arndt[3], Sabine Kasten[2,4], and Zijun Wu[1*]

[1]State Key Laboratory of Marine Geology, School of Ocean and Earth Science, Tongji University, Shanghai, 200092, P.R. China

[2]Alfred Wegener Institute Helmholtz Centre for Polar and Marine Research, 27570 Bremerhaven, Germany

[3]Department of Geosciences, Environment and Society, Universit´e Libre de Bruxelles, Avenue Franklin Roosevelt 50, 1050 Brussels, Belgium

[4]Faculty of Geosciences, University of Bremen, 28359 Bremen, Germany

*** Corresponding author. Email: wuzj@tongji.edu.cn**

https://doi.org/10.5194/bg-2022-228
Preprint. Discussion started: 25 November 2022

Abstract

Organic matter (OM) degradation in marine sediments is largely controlled by its reactivity and profoundly affects the global carbon cycle. Yet, there is currently no general framework that can constrain OM reactivity on a global scale. In this study, we propose a reactive continuum model based on a lognormal distribution (*l*-RCM) that is fully described by the mean μ and standard deviation σ of the sedimentary OM reactivity distribution. We use the *l*-RCM to inversely determine μ and σ at 123 sites across the global ocean. The results find that the apparent OM reactivity ($<k>=\mu \cdot \exp(\sigma^2/2)$) decreases with decreasing sedimentation rate (ω) and show that OM reactivity is more than three orders of magnitude higher in shelf than that in abyssal regions. Despite the general global trends, higher than expected OM reactivity is observed in certain deeper ocean regions, such as the Eastern-Western Coastal Equatorial Pacific and the Arabian Sea, emphasizing the complex control of the depositional environment (e.g., OM flux, oxygen content in the water column) on benthic OM reactivity. Notably, the *l*-RCM can also highlight the variability of OM reactivity in these regions. Based on inverse modeling results in our database, we establish the significant statistical relationships between $<k>$ and ω, and further map the global OM reactivity distribution.

1 Introduction

Marine sediments act as the ultimate sink for organic carbon. The size and reactivity of the benthic organic matter (OM) reservoir is a critical component of the global carbon cycle (Arndt et al., 2013). In particular, the reactivity of benthic OM imposes a substantial control on the magnitude of benthic carbon sequestration over geological timescales, the recycling

https://doi.org/10.5194/bg-2022-228
Preprint. Discussion started: 25 November 2022

of inorganic carbon and nutrients, the dissolution and precipitation of carbonates, the production of methane, and the activity of the seafloor biosphere (Dickens et al., 2004; Boudreau, 1992). Decades of research have shown that OM reactivity is controlled by both the nature of the OM (origin, composition and degradation state), as well as its environmental and depositional conditions (e.g., redox conditions, sedimentation rate, mineral protection, microbial community composition and biological mixing) (Burdige, 2007; Egger et al., 2018; Larowe et al., 2020a). However, due to the complex and dynamic nature of the main controls on OM reactivity, the specific relative significance of these controlling factors remains poorly quantified. Consequently, OM degradation models generally do not explicitly describe the influence of environmental and depositional factors on OM reactivity and its evolution but rather apply simplified parametrizations (Pika et al., 2021). Over the past decades, several models have been developed and successfully used to quantify OM degradation in marine sediments. They can be broadly divided into two groups: discrete models, such as the (multi) *G* model (Berner, 1964; Jørgensen, 1978), and continuum models, such as the reactive continuum model (RCM) and the power model (Boudreau and Ruddick, 1991; Middelburg, 1989).

Discrete models divide the bulk OM pool into a number of discrete fractions, each with its own constant reactivity. The 1-*G* model is the earliest OM degradation model. It is based on the assumption that OM degrades according to first order dynamics with a single constant degradation rate constant (Berner, 1964). The multi-*G* model, on the other hand, divides OM into several fractions, and each fraction is degraded according to a first-order rate with a fraction-specific reactivity (Jørgensen, 1978). Although multi-*G* models successfully fit observed OM degradation dynamics when comprehensive data sets are

https://doi.org/10.5194/bg-2022-228
Preprint. Discussion started: 25 November 2022

70 available, their application on a global scale is complicated by the need to partition the OM
71 reactivity into a finite number of fractions and define their reactivities. A multi-*G* model
72 with *n* discrete OM fractions requires constraining 2*n*-1 parameters and is, thus, over-
73 parametrized (Jørgensen, 1978). Nevertheless, because of its mathematical simplicity and
74 wide use, multi-*G* models have been used in a range of diagenetic models designed for the
75 global/regional scale (e.g., CANDI, MEDIA, MEDUSA, and OMEN SED) (Boudreau,
76 1996; Meysman et al., 2003; Munhoven, 2007; Pika et al., 2021). Constraining the 2*n*-1
77 OM degradation model parameters for these global-scale applications is not
78 straightforward. Early strategies for constraining the reactivity of OM on a global scale
79 have focused on deriving empirical relationships between OM reactivity and single, easily
80 observable characteristics of the depositional environment (water depth, sedimentation
81 rate, or OM flux) (Arndt et al., 2013). However, no statistically significant link between
82 OM reactivity and depositional environment could be established (R^2<0.1) after compiling
83 published multi-*G* models parameters across a wide range of depositional environments,
84 model complexities as well sediment depths/ burial time scales (Arndt et al., 2013).
85 Continuum models are an alternative to discrete models. They assume that OM
86 compounds are continuously distributed over a wide range of reactivities. The degradation
87 rate can be described as the sum of an infinite number of discrete fractions, each degraded
88 according to first-order kinetics (Boudreau and Ruddick, 1991), as
89 $$G(t) = \int_0^\infty G(0) \cdot g(k,0) \cdot e^{-kt} dk \quad (1)$$
90 where $G(t)$ is OM content at time t, $G(0)$ is OM content at the sediment-water interface
91 (SWI), k is the first-order degradation rate constant, and $g(k,0)$ is the initial reactivity
92 distribution of OM at the SWI. Boudreau and Ruddick(Boudreau and Ruddick, 1991),

https://doi.org/10.5194/bg-2022-228
Preprint. Discussion started: 25 November 2022

following Aris (Aris, 1968) and Ho *et al*. (Ho and Aris, 1987), proposed to use a Gamma distribution (γ-RCM) due to its mathematical properties and its ability to capture the observed dynamics:

$$g(k,0) = \frac{a^{\nu} \cdot k^{\nu-1} \cdot e^{-ak}}{\Gamma(\nu)} \quad (2)$$

where a is the average age of the OM at the SWI, ν is the shape parameter, and $\Gamma(\nu)$ is the Gamma function. In addition, Middelburg (Middelburg, 1989) empirically derived a power law from a large data compilation of measured OM reactivity, which is mathematically equivalent to the γ-RCM. The advantage of the continuum models over the discrete models is that they merely require constraining two free parameters to capture the widely observed continuous decrease in OM reactivity with degradation time/depth. Recently, γ-RCM has been used to inversely determine the free γ-RCM parameters, and thus benthic OM reactivity, from observed POC and sulfate depth profiles across a wide range of different depositional environments (Freitas et al., 2021). Although results revealed broad global patterns, no significant statistical relationship (R^2<0.46) between the parameters (a and ν) of the γ-RCM (Arndt et al., 2013) and characteristics of the depositional environment could be found, and constraining OM degradation model parameters on the global scale thus remains difficult.

Here, we present an RCM based on a lognormal distribution (l-RCM) (Forney and Rothman, 2012b):

$$g(k,0) = \frac{1}{k \cdot \sigma \cdot \sqrt{2\pi}} \cdot e^{-(\ln k - \ln \mu)^2/(2\sigma^2)} \quad (3)$$

where ln μ is the mean of ln k, and σ^2 is the variance of ln k (Fig. 1C). The lognormal distribution is commonly observed in nature (e.g., the radioactivity of elements in the crust, the incubation period of infectious diseases, ecological species abundance) (Limpert et al.,

https://doi.org/10.5194/bg-2022-228
Preprint. Discussion started: 25 November 2022

2001), and the rates of ocean primary production and biological carbon export also follow a lognormal distribution (Cael et al., 2018). In addition, inverse modeling of OM degradation data from 27 different types of litter, including leaves, wood, grass, and wheat, distributed across North America, ranging from the Alaskan tundra to the Panamanian rainforests, showed that OM reactivity followed a lognormal distribution (Forney and Rothman, 2012b). In this study, we use the *l*-RCM to simulate sedimentary OM profiles compiled from 123 sites covering the global depositional conditions. On this basis, we establish empirical relationships between OM reactivity versus sedimentation rate and further map the distribution of global sedimentary OM reactivity at the SWI.

2 Materials and methods

2.1 OM degradation model approach

The $g(k,0)$ we used in equation (1) is the lognormal distribution (equation (3)). Because of the tail of $g(k,0)$, the mean degradation rate or the apparent rate of the bulk OM ($<k>$) is greater than the median μ, as follows:

$$< k >= \int_0^\infty k \cdot g(k,0)dk = \mu \cdot e^{\sigma^2/2} \quad (4)$$

2.2 Inverse model approach

Here, we used 123 published datasets of OM depth profiles across a wide range of different depositional environments that have been sourced from published literature (Middelburg, 1989; Arndt et al., 2013; Middelburg et al., 1997) and the IODP database (Supplementary Fig. S1) to inversely determine the μ and σ parameters. We also analyzed a small number (n=12) of laboratory experiment data on OM degradation (Middelburg, 1989), as well as OM degradation data (n=16) from terrestrial soils (Katsev and Crowe, 2015). We followed the inverse modeling approach by Forney *et al.* (Forney and Rothman, 2012a) to identify

https://doi.org/10.5194/bg-2022-228
Preprint. Discussion started: 25 November 2022

the best-fitting parameters μ and σ based on the Newton method. We further improved this inverse method to reduce the influence of the initial value through nonlinear polynomial fitting using the least-squares method (Motulsky and Christopoulos, 2004).

2.3 Global upscaling of sedimentation rate

The inversely determined μ, σ couples of all investigated marine sites were then used in a linear regression method to derive the empirical relationships between OM parameters μ, σ, $<k>$ and the local sedimentation rates (ω). A correction factor was applied to account for the skewness bias inherent in the back conversion from a log-log transformed linear regression model to arithmetic units. The newly derived empirical relationships between $<k>$ and ω (Fig. 2) were then used to calculate global maps of OM reactivity at the SWI on a 1°×1° grid cell of the world ocean. At each grid point, ω were estimated based on the empirical relationship between ω (ω in cm yr^{-1}) and the water depth (z in m) (equation (5)), derived from 260 observations on the global continental shelves (Burwicz et al., 2011), complemented here by an extra 360 sites including abyss regions (data from Arndt *et al.* (Arndt et al., 2013), Egger *et al.* (Egger et al., 2018)).

$$\omega(z) = \frac{0.1}{1+\left(\frac{z}{200}\right)^{3.3}} + \frac{0.001}{1+\left(\frac{z}{4500}\right)^{11.4}} \quad (5)$$

2.4 Regional OM reactivity distribution at the SWI

Unfortunately, the OM depth profile has not been measured and compiled for the global seafloor at a suitable spatial resolution. The empirical equations we obtained for the depositional environment (ω) and OM reactivity can be used to assess the distribution of OM reactivity on a regional and global scale. In addition, the continuous distribution of OM reactivity over the reactivity spectrum, $F_i(k,0)$, provides crucial quantitative information on the degradation process and its evolution during burial.

https://doi.org/10.5194/bg-2022-228
Preprint. Discussion started: 25 November 2022

$$F_i(k,0) = \sum_{i=1}^{n} \frac{G_i(0)\cdot g_i(k,0)}{\sum_{i=1}^{n} G_i(0)} \quad (6)$$

where $G_i(0)$ is the content of OM at the SWI of each grid cell, and $g_i(k,0)$ is its reactivity distribution. Referring to Seiter *et al*. (Seiter et al., 2004), we divided the ocean into 30 regions based on the distribution of OM content in global marine surface sediments (Fig. 3). Using surface OM data at 5600 sites (Supplementary Fig. S11) (Seiter et al., 2004) and the relationship between water depth, μ, σ, and ω (Supplementary Fig. S9 and S10), we estimated the distribution of OM reactivity at the SWI, $F_i(k,0)$, in the 30 regions we divided (Supplementary Fig. S12).

We use a multi-*G* approximation method to calculate $<k_i>$ in each region (Bradley et al., 2020; Larowe et al., 2020b; Freitas et al., 2021). According to $F_i(k,0)$, the bulk OM at the SWI is divided into 1000 distinct fractions, and $<k_i>$ was calculated as:

$$< k >= \int_0^{\infty} k \cdot F_i(k,0)dk = \sum_{i=1}^{1000} f_i \cdot k_i \quad (7)$$

where f_i is the initial proportion of total OM in fraction *i*. The solution of f_i can be found in Supplementary equation (S3)–(S4).

3 Results and discussion

3.1 OM reactivity distribution based on the *l*-RCM and the γ-RCM

First, we determined the best fit to the eight OM datasets reported by Westrich *et al*. (Westrich and Berner, 1984), using the *l*-RCM and the γ-RCM. Both models fit the data equally well, as illustrated by the high coefficient of determination for each fit (R^2>0.9, Supplementary Fig. S3). However, the *l*-RCM and the γ-RCM differ in their ability to find a unique solution and in their respective probability density functions of OM reactivity ($\rho(k)$). For example, Fig. 1A and 1B show the best-fit OM profiles for two contrasting sites:

https://doi.org/10.5194/bg-2022-228
Preprint. Discussion started: 25 November 2022


Biogeosciences Discussions

185 BX-6 in the shelf and DSDP 58 in the abyssal region. The inversely determined parameters
186 at the two sites are μ=2.23×10^{-3} yr^{-1}, σ=2.03 at BX-6, and μ=6.11×10^{-5} yr^{-1}, σ=1.66 at DSDP
187 58 by the *l*-RCM. At BX-6, the best-fitting parameters by the γ-RCM are v =0.278 and
188 a=22.5, and at DSDP 58, v=1.08 and a=20224. According to the parameter sensitivity
189 analysis (Fig. 1D), the R^2 of the fitted results remains greater than 0.9 when a and v change
190 substantially simultaneously. As a result, different combinations of a and v can fit the data
191 equally well. For example, simultaneously increasing v and a (v=0.5 and a=53) at site BX-
192 6 or decreasing v and a (v=0.5 and a=4024) at site DSDP 58 lead to a slight change in R^2.
193 Freitas *et al.* (Freitas et al., 2021) showed that adding additional observational data, such
194 as porewater depth profiles, can help find a unique solution. In contrast, the best-fit
195 parameters μ and σ are unique in the *l*-RCM, and even small changes in either parameter
196 can lead to abysmal fitting results (Fig. 1D). The second difference between the two models
197 concerns the shape of the probability distribution $\rho(k)$. Statistically, the features of the
198 Gamma distribution vary with the value of v. It is divergent when v<1 and convergent when
199 v>1, making it difficult to visually compare the reactivity distributions of site BX-6 and
200 DSDP 58 (Fig. 1C). Compared to OM reactivity described by the γ-RCM, the *l*-RCM can
201 better distinguish OM reactivity distribution at different sites (Fig. 1C).

https://doi.org/10.5194/bg-2022-228
Preprint. Discussion started: 25 November 2022

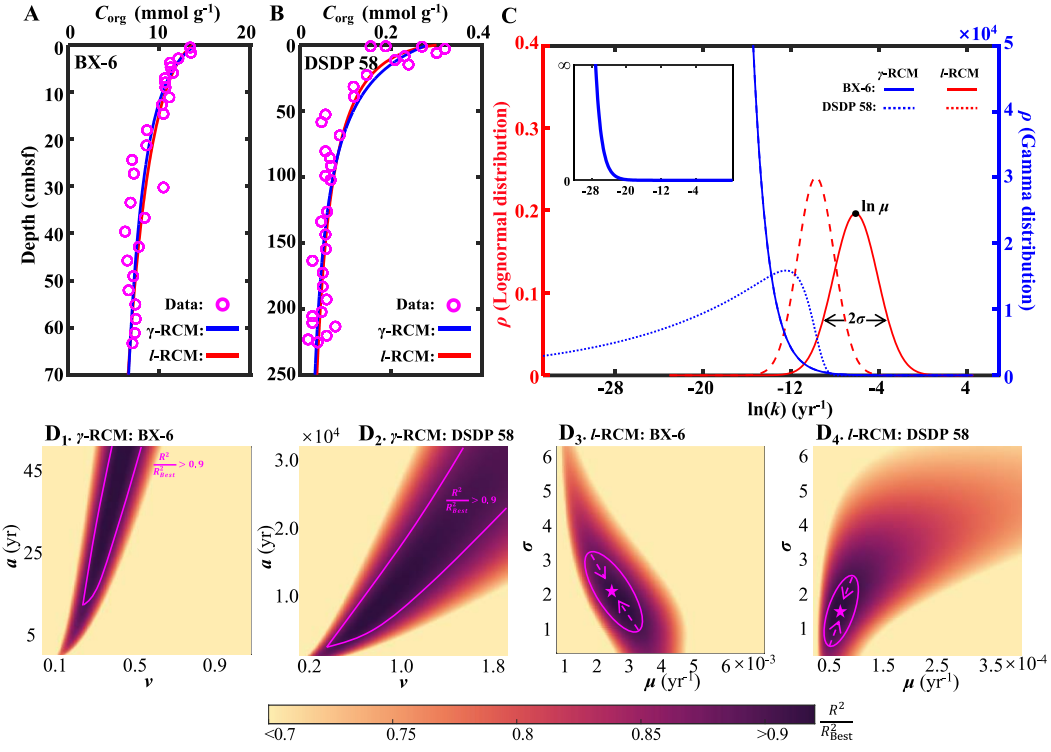

Figure 1. Comparison of *l*-RCM and *γ*-RCM. A, **B**, the fitting results of the *l*-RCM and the *γ*-RCM for site BX-6 and DSDP 58. **C**, OM reactivity distribution from *l*-RCM and *γ*-RCM. Top inset, Gamma distribution at site BX-6 at a larger y-axis. **D**, Distribution of R^2/R^2_{Best} for parameter sensitivity analysis of the *γ*-RCM and the *l*-RCM at sites BX-6 and DSDP 58. The pink lines in the D_1 and D_2 denote the range that R^2/R^2_{Best}>0.9 in the *γ*-RCM. The R^2/R^2_{Best} in the *l*-RCM converges as the pink arrows in the D_3 and D_4, ultimately reaching the best fitting results as the pink pentagrams.

3.2 Global distribution of OM reactivity

The inverse determination of the *l*-RCM parameters μ and σ across the wide range of different depositional environments allows quantitative insights into OM reactivity and provides essential information on the main environmental controls on OM reactivity. Fig. 2A illustrates the inversely determined μ-σ for all 123 depth profiles of marine sediment

https://doi.org/10.5194/bg-2022-228
Preprint. Discussion started: 25 November 2022

POC investigated in this study and compares them with inversely determined parameters from published soil and laboratory incubation data. It highlights the large inter- and intraregional variability of best-fit μ (10^{-6}–10^{2} yr^{-1}) and σ (0.2–6). However, despite the large variability, it also reveals broad global patterns in μ and σ and thus OM reactivity (<*k*>) (equation (4)). Notably, best-fit μ-σ couples form environmental clusters along a μ gradient, with the highest μ being determined for laboratory degradation experiments of fresh phytoplankton (Garber, 1984; Westrich and Berner, 1984) (μ=10^{0}–10^{2} yr^{-1}), followed by soil incubation under natural (Katsev and Crowe, 2015), yet still idealized conditions (μ=10^{0}–10^{1} yr^{-1}), while OM degraded in marine sediments generally reveals lower inversely determined μ<10^{0} yr^{-1}. The higher μ values determined for soil OM seemingly contradict the widely accepted notion that soil OM is generally less reactive than marine OM (Larowe et al., 2020a; Zonneveld et al., 2010). However, this apparent contradiction can be explained by the idealized conditions of the incubation experiments (e.g., only one type of material, some of which had nitrogen added), as well as the degradation state of the investigated OM. Although soil OM is structurally less reactive (Zonneveld et al., 2010; Hedges and Keil, 1995), the soil incubation experiments were conducted with initially undegraded material. In contrast, OM deposited in marine sediments consists of a complex mixture of OM from autochthonous and allochthonous sources that is altered to various degrees during transit from its source to the sediment (Hewson et al., 2012).

In addition to the difference between incubation data and field observations, Fig. 2A also reveals a three order of magnitude decrease in inversely determined μ for OM from the shelf (10^{-3}–10^{-1} yr^{-1}) to the slope (10^{-4}–10^{-3} yr^{-1}), and ultimately abyssal regions (<10^{-4} yr^{-1}). In addition, shelf and slope regions also generally reveal a larger σ (1–3), while abyssal

https://doi.org/10.5194/bg-2022-228
Preprint. Discussion started: 25 November 2022

239 regions display a narrower σ range (0.5–1). This observed progressive decrease in μ and σ
240 from the shelf to the abyssal ocean confirms previously observed patterns (Arndt et al.,
241 2013; Freitas et al., 2021; Zonneveld et al., 2010) and reflects the interaction between OM
242 structure (or its source) and the degree of alteration/pre-processing as OM transits from its
243 original source to the ultimate sedimentary sink. In the dynamic shelf regions, highly
244 variable OM loads from different sources, including *in*-situ produced marine OM, laterally
245 transported, pre-processed terrestrial or marine OM, are often physically protected from
246 further erosion/deposition cycles due to high suspended sediment loads (Arndt et al., 2013;
247 Larowe et al., 2020a). As a result, benthic OM is composed of a complex mixture of fresh
248 and pre-aged compounds of highly variable (hence larger σ of the initial distribution), yet
249 generally higher reactivity. On the upper and mid-continental slopes, intensive lateral
250 and/or vertical transport processes or the abrupt relocation of sediment result in similar
251 complex mixtures of OM (hence similar σ of the initial distribution) (Larowe et al., 2020a).
252 However, transport timescales are often longer due to the greater water depths and distance
253 to land. The deposited OM is generally more degraded and thus less reactive than in shelf
254 environments. In contrast, benthic OM in abyssal regions is mainly derived from marine
255 production (Rowe and Staresinic, 1979; Larowe et al., 2020a). During its slow settling
256 through the water column, highly reactive OM compounds are rapidly degraded, and only
257 the less reactive compounds persist and settle onto the sediment (Dunne et al., 2007). The
258 values of μ and σ in the abyssal regions are thus significantly smaller than in the shelf and
259 slope regions. Especially in the NE-Pacific (NEPAC) region, deeper water depth
260 (>5000m), relatively low OM content (~0.2wt.%), and the old OM age (>10^4 years) result
261 in comparably lower μ and σ values (Fig. 2A) and, thus, extremely low benthic OM

https://doi.org/10.5194/bg-2022-228
Preprint. Discussion started: 25 November 2022

262 reactivity (Müller and Suess, 1979). The decrease of μ and σ from the shelf to abyssal
263 regions reveals a decline in reactivity during lateral transport of OM, where μ mainly
264 controls the overall reactivity and σ indicates the coverage of the main component of OM.
265 Fig. 2B shows the global trend of OM reactivity (<*k*>) with sedimentation rate (ω),
266 which is a widely observed and comparably easy to measure proxy for local depositional
267 conditions with sizable global data sets or empirical formulas available (Burwicz et al.,
268 2011). In addition, Fig. 2B further reveals a general decreasing trend in <*k*> *vs* ω, and a
269 good regression (R^2=0.78) for the general sea regions (shelf (<200m), slope (200–2000m),
270 and abyss (>2000m)). However, the general trend is superimposed by a large variability
271 and apparent reactivity <*k*> in specific environments, notably deviating from this generally
272 observed trend. More specifically, higher μ and σ values and, thus, higher OM reactivities
273 occur in the Eastern-Western Coastal Equatorial Pacific (EWEP), Southwestern-Africa
274 continental margin (SWAF), Northwestern-America continental margin (NWAM), and the
275 Arabian Sea (ARBS) regions. These results are completely consistent with prior
276 observations and model results (Arndt et al., 2013) and can be directly linked to the
277 prevailing depositional conditions. High benthic OM reactivities have previously been
278 reported for depositional environments that are characterized by a dominance of marine
279 algal OM (e.g., EWEP) (Hammond et al., 1996), strong lateral transport processes (e.g.,
280 SWAF, NWAM)(Arndt et al., 2013). Furthermore, the reactivity of sedimentary OM is
281 considerably influenced by oxygen content or more precisely, by oxygen exposure time in
282 the water column and the bottom water (Aller, 1994; Hartnett et al., 1998; Hedges and Keil,
283 1995; Mollenhauer et al., 2003; Zonneveld et al., 2010). Lower oxygen concentrations, as
284 present in these regions in the form of pronounced oxygen minimum zones, will slow down

https://doi.org/10.5194/bg-2022-228
Preprint. Discussion started: 25 November 2022

285 the degradation of OM both in the water column and at the sediment surface. This enables
286 the burial of more reactive OM into the sediments and thus results in the occurrence of
287 high sedimentary OM reactivity in these regions despite great water depth (Arndt et al.,
288 2013; Bogus et al., 2012; Ingole et al., 2010; Luff et al., 2000; Volz et al., 2018). Our
289 approach predicts higher OM reactivity in the Arabian Sea (ARBS) with deep water depth,
290 that is consistent with the observation of one of the most pronounced ocean oxygen
291 minimum zones in this region due to strong coastal upwelling or a high export rate of
292 plankton-derived OM into the underlying water column. The *l*-RCM captures the broad
293 patterns of OM reactivity across the global seafloor even better than previous models and
294 also provides statistically more significant relationships between OM reactivity (<*k*>) and
295 sedimentation rate (ω) than inversely determined parameters of γ-RCM (R^2<0.46) and
296 discrete models (R^2<0.1)(Arndt et al., 2013). Although the relationship between <*k*> and
297 ω for special regions (e.g., EWEP, SWAF, NWAM, and ARBS) is less quality, it still
298 provides an excellent first-order predictor and a step forward in assessing broad global
299 patterns in OM reactivity.
300

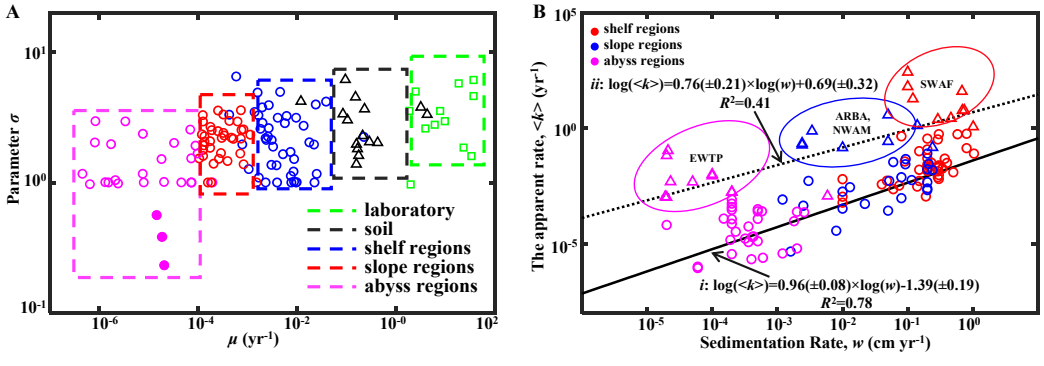

301

https://doi.org/10.5194/bg-2022-228
Preprint. Discussion started: 25 November 2022

Figure 2. Global distribution of OM reactivity. A, Distribution of parameters σ and μ in different regions. Pink solid circles denote fitting results of sites in the NEPAC with extremely low OM reactivity. **B**, Log-log plot of ω and $<k>$. The solid black line (*i*) denotes linear regression for shelf, slope, and abyss regions. The black dotted line (*ii*) denotes linear regression for high OM reactivity regions, including the EWTP, ARBS, NWAM, and SWAF regions.

3.3 Implication of Global OM reactivity patterns

Considering the geographic differences in depositional environments and in order to describe the global distribution of sedimentary OM reactivity in more detail, we divided the global ocean into 30 different regions using 5600 single measured data of OM content in global surface sediment (<5 cm sediment depth) and the previously used combined qualitative and quantitative geostatistical methods (Seiter et al., 2004). Based on the empirical $<k>$–ω relationships in Fig. 2B (*i* for the general water depth-related regions, *ii* for the specific regions (EWTP, ARBS, NWAM, and SWAF)), and the water depth–ω relationship (equation (5)), we finally derived, to our knowledge, the world's first map of the apparent reactivity of sedimentary OM distribution in the global ocean (Fig. 3).

https://doi.org/10.5194/bg-2022-228
Preprint. Discussion started: 25 November 2022

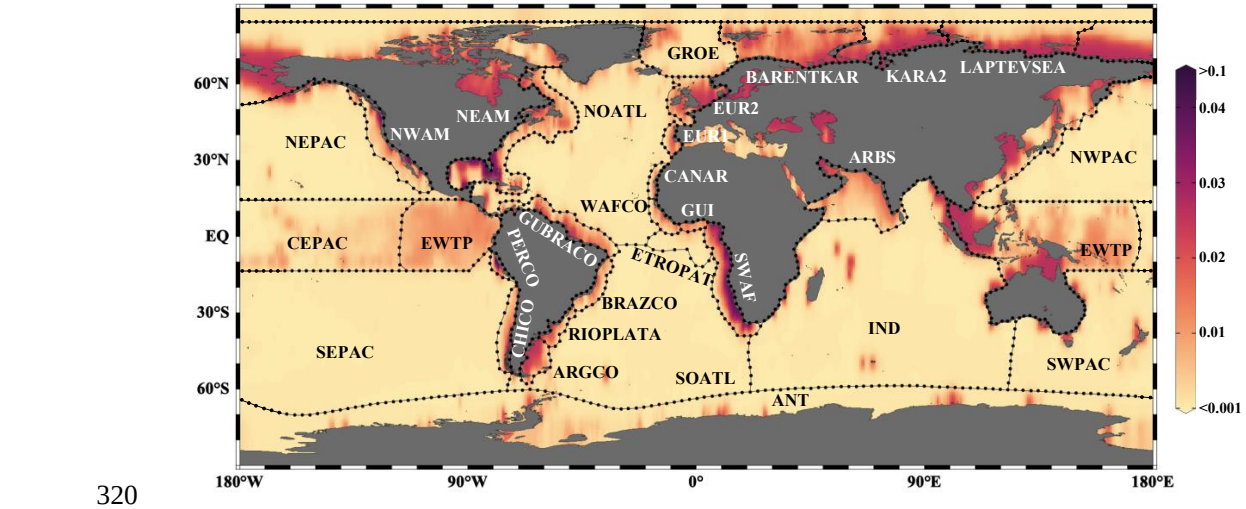

Figure 3. Distribution of <*k*> (yr^{-1}) at the SWI in the global ocean with 1°×1° resolution and the 30 regions we divided of the global ocean. The abbreviations of the 30 regions we divided are defined in Table 1.

Given OM degradation is closely related to its reactivity, this map has potentially important applications for quantitative evaluation of the global OM degradation in sediments and its related carbon budget. Previous work estimated the global budget of OM degradation by the *G*-model or the *γ*-RCM from 1.314 Pg C yr^{-1} to 3.127 Pg C yr^{-1}, with ~85% occurring in the shelf regions (Jørgensen, 1983; Larowe et al., 2020b; Middelburg et al., 1997; Smith and Hollibaugh, 1993). However, the *γ*-RCM describes the global-scale OM reactivity patterns by a single empirical equation of parameters *a*-*ω* and parameter *v* in a smaller range (0.1–0.2) (Larowe et al., 2020b; Arndt et al., 2013; Bradley et al., 2020) and poor statistical relationship between the *G*-model parameters and depositional environment, thus leading to underestimating OM degradation in special regions, particularly in the EWTP, with large area and higher OM reactivity (Table 1, Fig. 3). In addition, OM reactivity governs benthic biogeochemical cycling and exchange (Freitas et

https://doi.org/10.5194/bg-2022-228
Preprint. Discussion started: 25 November 2022

337 al., 2021), and the dissolved inorganic carbon (DIC) generation via benthic OM
338 degradation has a significant impact on ocean acidification and atmospheric CO_2 levels
339 (Krumins et al., 2013). Therefore, the *l*-RCM can be further used to calculate the budget of
340 OM degradation at regional or global scales and assess the significance of the sedimentary
341 carbon cycle on the hydrosphere and atmosphere.

342

343

Table 1 Abbreviations of regions in this paper, and their area, mean OM content in surface sediment (<5 cm), and <*k*>.

Abbreviation	Region	Seafloor area[a]	Mean OM[b]	<*k*>[c]
		($\times 10^{12}$ m^2)	(wt.%)	(yr^{-1})
SWAF	Southwestern-Africa continental margin	0.8	2.5	0.50936
NWAM	Northwestern-America continental margin	0.5	1.7	0.13596
ARBS	Arabian Sea	3.9	1.4	0.10302
EWTP	Eastern-Western Coastal Equatorial Pacific	35.1	1.2	0.00173
ANT	South Polar Sea	24.2	0.3	0.02557
ARGCO	Argentina continental margin	0.8	0.3	0.00020
BARENTKAR	Barents Sea and Kara Sea	1.7	1.1	0.02413
BRAZCO	Brazil continental margin	1.1	0.5	0.02662
CANAR	Canaries	0.6	0.6	0.01073
CEPAC	Central Equatorial Pacific	30.9	0.3	0.00004
CHICO	Chile continental margin	0.8	1.5	0.01620
ETROPAT	Eastern tropical Atlantic	1.8	0.7	0.00828
EUR1	Northern-European continental margin	2.3	0.8	0.03132
EUR2	Southern-European continental margin	1.7	0.3	0.02176
GROE	Northern Nordic Sea	4.8	0.7	0.00445
GUBRACO	Southeastern-America continental margin	1.6	0.4	0.02462
GUI	Gulf of Guinea	0.3	1.1	0.02678
INA	Indian Ocean deep sea	54.9	0.4	0.00012
KARA2	Kara Sea	1.6	1.2	0.03685
LAPTEVSEA	Laptev Sea	2.1	0.9	0.05052
NEAM	Northeastern-America continental margin	5.2	0.9	0.02907
NEPAC	Northeastern-Pacific	24.9	0.4	0.00011
NOATL	Northern Atlantic	30.3	0.4	0.00014
NWPAC	Northwestern-Pacific	15.6	0.6	0.00007
PERCO	Peru continental margin	0.6	4.8	0.01244

https://doi.org/10.5194/bg-2022-228
Preprint. Discussion started: 25 November 2022

RIOPLATA	Rio de la Plata mouth	0.7	0.8	0.00778
SEPAC	Southeastern-Pacific	49.6	0.5	0.00018
SOATL	Southern Atlantic	39.3	0.4	0.00013
SWPAC	Southwestern-Pacific	22.3	0.8	0.00017
WAFCO	Western-Africa continental margin	0.9	0.6	0.00017

[a]The total ocean area covered in this study equals 3.60×10^8 km^2, corresponding to ~99% of the total ocean. [b]Mean OM data were collected from Seiter *et al*. (Seiter et al., 2004). [c]See equation (7) for the solution of $<k>$ in each region.

4 Conclusions

Compared with the previous OM degradation models, the *l*-RCM not only well fits OM depth-profiles, but also better represents the distribution of OM reactivity by the parameters μ and σ. We use the *l*-RCM to inversely determine μ and σ at 123 sites across the global ocean, including the shelf, slope and abyss regions. Our results show that the apparent OM reactivity ($<k>=\mu\cdot\exp(\sigma^2/2)$) decreases with decreasing sedimentation rate (ω), and OM reactivity is more than three orders of magnitude higher in shelf than that in abyssal regions. Due to the complex depositional environments, such as oxygen minimum zones caused by strong coastal upwelling or a high export rate of plankton-derived OM into the underlying water column, OM reactivity is higher than predicted in some specific regions (e.g., the NWAM, SWAF, ARBS, and EWTP regions), yet the *l*-RCM can still capture OM reactivity features in these regions. Based on two empirical relationships between the OM reactivity ($<k>$) and sedimentation rate (ω), we obtained the global OM reactivity distribution patterns and finally mapped the global OM reactivity distribution for the first time. Overall, our *l*-RCM can potentially be used to calculate the budget of OM degradation at regional or global scales and assess the significance of the sedimentary carbon cycle on the hydrosphere and atmosphere.

https://doi.org/10.5194/bg-2022-228
Preprint. Discussion started: 25 November 2022

363

364

365 **References**

366 Aller, R. C.: Bioturbation and remineralization of sedimentary organic matter: effects of
367 redox oscillation, Chem Geol, 114, 331-345, doi:10.1016/0009-2541(94)90062-0,
368 1994.
369 Aris, R.: Prolegomena to the rational analysis of systems of chemical reactions II. Some
370 addenda, Archive for Rational Mechanics and Analysis, 27, 356-364,
371 doi:10.1007/BF00282276, 1968.
372 Arndt, S., Jørgensen, B. B., LaRowe, D. E., Middelburg, J., Pancost, R., and Regnier, P.:
373 Quantifying the degradation of organic matter in marine sediments: a review and
374 synthesis, Earth-science reviews, 123, 53-86, doi:10.1016/j.earscirev.2013.02.008,
375 2013.
376 Berner, R. A.: An idealized model of dissolved sulfate distribution in recent sediments,
377 Geochimica et Cosmochimica Acta, 28, 1497-1503, doi:10.1016/0016-7037(64)90164-
378 4, 1964.
379 Bogus, K. A., Zonneveld, K. A., Fischer, D., Kasten, S., Bohrmann, G., and Versteegh, G.
380 J.: The effect of meter-scale lateral oxygen gradients at the sediment-water interface on
381 selected organic matter based alteration, productivity and temperature proxies,
382 Biogeosciences, 9, 1553-1570, doi:10.5194/bg-9-1553-2012, 2012.
383 Boudreau, B. P.: A kinetic model for microbic organic-matter decomposition in marine
384 sediments, FEMS microbiology ecology, 11, 1-14, doi:10.1111/j.1574-
385 6968.1992.tb05789.x, 1992.
386 Boudreau, B. P.: A method-of-lines code for carbon and nutrient diagenesis in aquatic
387 sediments, Computers & Geosciences, 22, 479-496, doi:10.1016/0098-
388 3004(95)00115-8, 1996.
389 Boudreau, B. P. and Ruddick, B. R.: On a reactive continuum representation of organic
390 matter diagenesis, American Journal of Science, 291, 507-538,
391 doi:10.2475/ajs.291.5.507, 1991.
392 Bradley, J., Arndt, S., Amend, J., Burwicz, E., Dale, A. W., Egger, M., and LaRowe, D.
393 E.: Widespread energy limitation to life in global subseafloor sediments, Science
394 advances, 6, doi:10.1126/sciadv.aba0697, 2020.
395 Burdige, D. J.: Preservation of organic matter in marine sediments: controls, mechanisms,
396 and an imbalance in sediment organic carbon budgets?, Chem Rev, 107, 467-485,
397 doi:10.1021/cr050347q, 2007.
398 Burwicz, E. B., Rüpke, L., and Wallmann, K.: Estimation of the global amount of
399 submarine gas hydrates formed via microbial methane formation based on numerical
400 reaction-transport modeling and a novel parameterization of Holocene sedimentation,
401 Geochimica et Cosmochimica Acta, 75, 4562-4576, doi:10.1016/j.gca.2011.05.029,
402 2011.
403 Cael, B., Bisson, K., and Follett, C. L.: Can rates of ocean primary production and
404 biological carbon export be related through their probability distributions?, Global
405 biogeochemical cycles, 32, 954-970, doi:10.1029/2017GB005797, 2018.

https://doi.org/10.5194/bg-2022-228
Preprint. Discussion started: 25 November 2022

406 Dickens, A. F., Gelinas, Y., Masiello, C. A., Wakeham, S., and Hedges, J. I.: Reburial of
407 fossil organic carbon in marine sediments, Nature, 427, 336-339,
408 doi:10.1038/nature02299, 2004.
409 Dunne, J. P., Sarmiento, J. L., and Gnanadesikan, A.: A synthesis of global particle export
410 from the surface ocean and cycling through the ocean interior and on the seafloor, Global
411 Biogeochemical Cycles, 21, doi:10.1029/2006GB002907, 2007.
412 Egger, M., Riedinger, N., Mogollón, J. M., and Jørgensen, B. B.: Global diffusive fluxes
413 of methane in marine sediments, Nature Geoscience, 11, 421-425,
414 doi:10.1038/s41561-018-0122-8, 2018.
415 Forney, D. and Rothman, D.: Inverse method for estimating respiration rates from decay
416 time series, Biogeosciences, 9, 3601-3612, doi:10.5194/bg-9-3601-2012, 2012a.
417 Forney, D. C. and Rothman, D. H.: Common structure in the heterogeneity of plant-matter
418 decay, Journal of The Royal Society Interface, 9, 2255-2267,
419 doi:10.1098/rsif.2012.0122, 2012b.
420 Freitas, F. S., Pika, P. A., Kasten, S., Jørgensen, B. B., Rassmann, J., Rabouille, C.,
421 Thomas, S., Sass, H., Pancost, R. D., and Arndt, S.: Advancing on large-scale trends of
422 apparent organic matter reactivity in marine sediments and patterns of benthic carbon
423 transformation, Biogeosciences Discussions, 2021, 1-64, doi:10.5194/bg-18-4651-2021,
424 2021.
425 Garber, J. H.: Laboratory study of nitrogen and phosphorus remineralization during the
426 decomposition of coastal plankton and seston, Estuarine, Coastal and Shelf Science, 18,
427 685-702, doi:10.1016/0272-7714(84)90039-8, 1984.
428 Hammond, D., McManus, J., Berelson, W., Kilgore, T., and Pope, R.: Early diagenesis of
429 organic material in equatorial Pacific sediments: stpichiometry and kinetics, Deep Sea
430 Research Part II: Topical Studies in Oceanography, 43, 1365-1412, doi:10.1016/0967-
431 0645(96)00027-6, 1996.
432 Hartnett, H. E., Keil, R. G., Hedges, J. I., and Devol, A. H.: Influence of oxygen exposure
433 time on organic carbon preservation in continental margin sediments, Nature,
434 391(6667), 572-575, doi:10.1038/35351, 1998.
435 Hedges, J. I. and Keil, R. G.: Sedimentary organic matter preservation: an assessment and
436 speculative synthesis, Marine chemistry, 49, 81-115, doi:10.1016/0304-4203(95)00008-
437 F, 1995.
438 Hewson, I., Barbosa, J. G., Brown, J. M., Donelan, R. P., Eaglesham, J. B., Eggleston, E.
439 M., and LaBarre, B. A.: Temporal dynamics and decay of putatively allochthonous and
440 autochthonous viral genotypes in contrasting freshwater lakes, Applied and
441 environmental microbiology, 78, 6583-6591, doi:10.1128/AEM.01705-12, 2012.
442 Ho, T. and Aris, R.: On apparent second-order kinetics, AIChE journal, 33, 1050-1051,
443 doi:10.1002/aic.690330621, 1987.
444 Ingole, B. S., Sautya, S., Sivadas, S., Singh, R., and Nanajkar, M.: Macrofaunal community
445 structure in the western Indian continental margin including the oxygen minimum zone,
446 Marine Ecology, 31, 148-166, doi:10.1111/j.1439-0485.2009.00356.x, 2010.
447 Jørgensen, B.: A comparison of methods for the quantification of bacterial sulfate reduction
448 in coastal marine sediments. II. Calculation from mathematical models, Geomicrobiol.
449 J, 1, 29-47, 10.1080/01490457809377721, doi:10.1080/01490457809377721, 1978.
450 Jørgensen, B.: Processes at the sediment-water interface, The major biogeochemical cycles
451 and their interactions, 477-509, 1983.

https://doi.org/10.5194/bg-2022-228
Preprint. Discussion started: 25 November 2022

452 Katsev, S. and Crowe, S. A.: Organic carbon burial efficiencies in sediments: The power
453 law of mineralization revisited, Geology, 43, 607-610, doi:10.1130/G36626.1, 2015.
454 Krumins, V., Gehlen, M., Arndt, S., Van Cappellen, P., and Regnier, P.: Dissolved
455 inorganic carbon and alkalinity fluxes from coastal marine sediments: model estimates
456 for different shelf environments and sensitivity to global change, Biogeosciences, 10,
457 371-398, doi:10.5194/bg-10-371-2013, 2013.
458 LaRowe, D., Arndt, S., Bradley, J., Estes, E., Hoarfrost, A., Lang, S., Lloyd, K.,
459 Mahmoudi, N., Orsi, W., and Walter, S. S.: The fate of organic carbon in marine
460 sediments-New insights from recent data and analysis, Earth-Science Reviews, 204,
461 103146, doi:10.1016/j.earscirev.2020.103146, 2020a.
462 LaRowe, D. E., Arndt, S., Bradley, J. A., Burwicz, E., Dale, A. W., and Amend, J. P.:
463 Organic carbon and microbial activity in marine sediments on a global scale throughout
464 the Quaternary, Geochimica et Cosmochimica Acta, 286, 227-247,
465 doi:10.1016/j.gca.2020.07.017, 2020b.
466 Limpert, E., Stahel, W. A., and Abbt, M.: Log-normal distributions across the sciences:
467 keys and clues: on the charms of statistics, and how mechanical models resembling
468 gambling machines offer a link to a handy way to characterize log-normal distributions,
469 which can provide deeper insight into variability and probability—normal or log-
470 normal: that is the question, BioScience, 51, 341-352, doi:10.1641/0006-
471 3568(2001)051[0341:LNDATS]2.0.CO;2, 2001.
472 Luff, R., Wallmann, K., Grandel, S., and Schlüter, M.: Numerical modeling of benthic
473 processes in the deep Arabian Sea, Deep Sea Research Part II: Topical Studies in
474 Oceanography, 47, 3039-3072, doi:10.1016/S0967-0645(00)00058-8, 2000.
475 Meysman, F. J., Middelburg, J. J., Herman, P. M., and Heip, C. H.: Reactive transport in
476 surface sediments. II. Media: an object-oriented problem-solving environment for early
477 diagenesis, Computers & geosciences, 29, 301-318, doi:10.1016/S0098-
478 3004(03)00007-4, 2003.
479 Middelburg, J. J.: A simple rate model for organic matter decomposition in marine
480 sediments, Geochimica et Cosmochimica acta, 53, 1577-1581, 10.1016/0016-
481 7037(89)90239-1, doi:10.1016/0016-7037(89)90239-1, 1989.
482 Middelburg, J. J., Soetaert, K., and Herman, P. M.: Empirical relationships for use in global
483 diagenetic models, Deep Sea Research Part I: Oceanographic Research Papers, 44, 327-
484 344, doi:10.1016/S0967-0637(96)00101-X, 1997.
485 Mollenhauer, G., Eglinton, T. I., Ohkouchi, N., Schneider, R. R., Müller, P. J., Grootes, P.
486 M., and Rullkötter, J.: Asynchronous alkenone and foraminifera records from the
487 Benguela Upwelling System, Geochimica et cosmochimica acta, 67, 2157-2171,
488 doi:10.1016/S0016-7037(03)00168-6, 2003.
489 Motulsky, H. and Christopoulos, A.: Fitting models to biological data using linear and
490 nonlinear regression: a practical guide to curve fitting, Oxford University Press2004.
491 Müller, P. J. and Suess, E.: Productivity, sedimentation rate, and sedimentary organic
492 matter in the oceans—I. Organic carbon preservation, Deep Sea Research Part A.
493 Oceanographic Research Papers, 26, 1347-1362, doi:10.1016/0198-0149(79)90003-7,
494 1979.
495 Munhoven, G.: Glacial–interglacial rain ratio changes: Implications for atmospheric CO2
496 and ocean–sediment interaction, Deep Sea Research Part II: Topical Studies in
497 Oceanography, 54, 722-746, doi:10.1016/j.dsr2.2007.01.008, 2007.

https://doi.org/10.5194/bg-2022-228
Preprint. Discussion started: 25 November 2022

498 Pika, P., Hülse, D., and Arndt, S.: OMEN-SED (-RCM)(v1. 1): a pseudo-reactive
499 continuum representation of organic matter degradation dynamics for OMEN-SED,
500 Geoscientific Model Development, 14, 7155-7174, doi:10.5194/gmd-14-7155-2021,
501 2021.
502 Rowe, G. T. and Staresinic, N.: Sources of organic matter to the deep-sea benthos, Ambio
503 Special Report, 19-23, doi:10.2307/25099603, 1979.
504 Seiter, K., Hensen, C., Schröter, J., and Zabel, M.: Organic carbon content in surface
505 sediments—defining regional provinces, Deep Sea Research Part I: Oceanographic
506 Research Papers, 51, 2001-2026, doi:10.1016/j.dsr.2004.06.014, 2004.
507 Smith, S. and Hollibaugh, J.: Coastal metabolism and the oceanic organic carbon balance,
508 Reviews of Geophysics, 31, 75-89, doi:10.1029/92RG02584, 1993.
509 Volz, J. B., Mogollón, J. M., Geibert, W., Arbizu, P. M., Koschinsky, A., and Kasten, S.:
510 Natural spatial variability of depositional conditions, biogeochemical processes and
511 element fluxes in sediments of the eastern Clarion-Clipperton Zone, Pacific Ocean, Deep
512 Sea Research Part I: Oceanographic Research Papers, 140, 159-172,
513 doi:10.1016/j.dsr.2018.08.006, 2018.
514 Westrich, J. T. and Berner, R. A.: The role of sedimentary organic matter in bacterial
515 sulfate reduction: The G model tested 1, Limnology and oceanography, 29, 236-249,
516 doi:10.4319/lo.1984.29.2.0236, 1984.
517 Zonneveld, K. A., Versteegh, G. J., Kasten, S., Eglinton, T. I., Emeis, K.-C., Huguet, C.,
518 Koch, B. P., de Lange, G. J., de Leeuw, J. W., and Middelburg, J. J.: Selective
519 preservation of organic matter in marine environments; processes and impact on the
520 sedimentary record, Biogeosciences, 7, 483-511, doi:10.5194/bg-7-483-2010, 2010.
521

522 **Acknowledges**

523 This study was supported by National Key Basic Research and Development Program of
524 China (2016YFA0601100), the Natural Science Foundation of China (41976057). Sinan
525 Xu gratefully acknowledges the financial support by the China Scholarship Council
526 (contract N. 201906260048) for a research stay at AWI, Germany.

527 **Author contributions**

528 S.X. and B.L. designed the study and performed the research with S.A., S.K., and Z.W.;

529 All authors discussed the results and commented on the manuscript.

530 **Competing interests**

531 The authors declare that they have no competing interests.